Progress In Electromagnetics Research, Vol. 140, 131–146, 2013

ANALYTICAL DESIGN AND FEM VERIFICATION OF A NOVEL THREE-PHASE SEVEN LAYERS SWITCHED RELUCTANCE MOTOR

Ebrahim Afjei[1, *], Alireza Siadatan[1], and Hossein Torkaman[2]

[1]Faculty of Electrical Engineering, Shahid Beheshti University, G.C., Tehran, Iran

[2]Faculty of Electrical and Computer Engineering, Power and Water University of Technology (Shahid Abbaspour University of Technology), Tehran, Iran

Abstract—The purpose of this paper is to propose analytical and finite element method (FEM) designs of a novel three-phase Seven Layers Switched Reluctance Motor (SLSRM) for the applications which dictated by the performance with the total torque per volume as a key marker indicator. The introduced motor consists of seven magnetically independent stator layers, which each layer includes a set of 4 by 4 stator/rotor poles. In this SLSRM, the three layers are energized together to produce high torque and also decrease the torque ripple in comparison with the one layer conventional SRM. Since each layer has its independent phase in the motor, the isolation problem of coils and cooling troublesome existing in conventional SRMs is solved. In addition, these types of SLSRM have some other advantages, like simpler configuration, cooling in easier way, etc.. Firstly an analytical design is carried out to illustrate the design procedure and then three-dimensional (3-D) magneto static simulation analysis of the SLSRM and the one layer SRM is performed using 3-D FEM, to obtain and verify the flux-linkage, flux density and torque profiles. Also, the proposed motor is compared with a conventional one layer SRM with a same size and volume.

Received 7 April 2013, Accepted 3 May 2013, Scheduled 29 May 2013

* Corresponding author: Ebrahim Afjei (e-afjei@sbu.ac.ir).

1. INTRODUCTION

Switched Reluctance Motor (SRM) is a strong motor which is taken into consideration by industries. It has high efficiency, needs low maintenances and can work in harsh environment. This type of motor is one of the challengers for low cost and simple structure in variable speed drive applications such hybrid electric vehicles, household appliances, and wind energy [1–5].

Generally speaking, there are two kinds of SRMs; Linear SRM (L-SRM) and the Rotary SRM (R-SRM). Based on this category, the general classification of SRM is shown in Figure 1.

Optimal design of different types of SRMs involve the selection of the motor's geometrical parameters to produce high output torque respects to its volume with considering the minimum ripples [6, 7]. Therefore, the efficient design of SRM is a considerable way to achieve high performance and output torque [8]. The efficient design of SRM has been undertaken based on various aspects as; (I) Modification of the rotor, stator shapes [9]; for instance; Double-layer per phase isolated and multilayer SRMs are introduced in [10] by authors to improve the torque ripple and noise with considering the maximum performance. (II) The use of numerical methods to efficient design and analysis process such as finite element method [11, 12]. (III) The intelligent and heuristics methods namely as Neural Network (NN) [13, 14], and Genetic algorithm (GA) [15, 16] play important role in the mentioned purpose of design. (IV) Optimum design of control and derive unites of motor [17–20].

Efficient and Optimal design of SRM for high performance motion control systems requires accurate knowledge of the magneto static fields that relate motor geometry and motor performance [21–23].

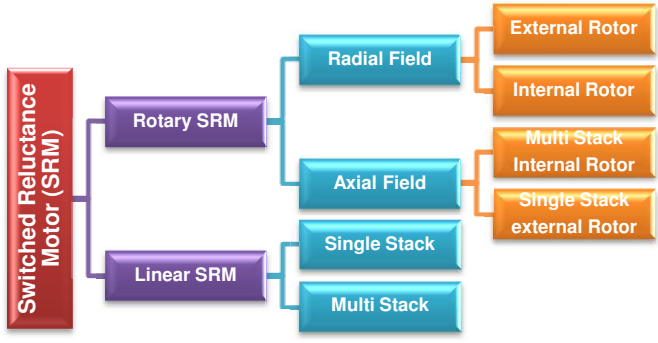

Figure 1. SRM classification.

These contexts can be explored through extensive prototyping, which is impractical and very costly, or by accurate magnetic field simulations. Magnetic field simulation directly yields predictions of flux linkages, field energy, and torque profiles

This paper investigates the design consideration of a novel type of switched reluctance motor, which its characteristic and profile are verified with numerical verification in next sections.

2. ANALYTICAL DESIGN PROCEDURE

The designing procedure is explained step by step as follows. The first step of SRM design is to determine the required output power P_{hp} and speed, which are;

$$P_{hp} = 2\,\text{hp}, \quad n = 1500\,\text{rpm}, \quad i_p = 12\,\text{A}, \quad n_s, n_r = 4$$

where i_p, n_s and n_r are the peak value of current, number of stator and rotor poles. The torque of the machine is calculated as:

$$T_{eq} = \frac{P_{hp}}{2\pi\left(\frac{N}{60}\right)} = \frac{2 \times 746}{2\pi\left(\frac{1500}{60}\right)} = 9.49\,\text{N} \cdot \text{m} \tag{1}$$

From the NEMA table the frame size for a 2 hp is selected based on IEC standard as:

$$\text{No. of fram size} = 56 \tag{2}$$

$$D = (3.5\,\text{inch}) \times 2.54 = 88.9\,\text{m} \tag{3}$$

The outer diameter of the stator is

$$D_0 = (88.9 - 3) \times 2 = 171.8\,\text{mm} \tag{4}$$

Because of the same ratio of L respect to D, thus the stack length L is:

$$L = D_0 = 171.8\,\text{mm} \quad \rightarrow \quad L \approx 170\,\text{mm} \tag{5}$$

Based on mentioned standard, for selected frame size, the maximum value of shaft diameter is calculated as

$$D_{sh} = \frac{5}{8}(\text{inch}) = 16\,\text{mm} \tag{6}$$

Air gap length is considered as (according to the manufacturing limitations)

$$g = 0.5\,\text{mm} \tag{7}$$

Based on B-H curve for selected core material, the maximum value of magnetic field intensities is put as:

$$B_{\max} = 1.8\,\text{T} \tag{8}$$

And the value of magnetic field intensities in the stator pole is also:

$$B_s = 1.8\,\mathrm{T} \tag{9}$$

The stator pole area A_s can be written as,

$$A_S = \frac{88.9}{2} \times 170 \times 45^\circ \times \frac{\pi}{180} = 5931.85 \times 10^{-6} = 5.93185 \times 10^{-3}\,\mathrm{m}^2 \tag{10}$$

The flux in the stator pole φ_s is,

$$\varphi_s = 1.8 \times 5931.85 \times 10^{-6} = 10.6773\,\mathrm{mWb} \tag{11}$$

The flux in the yoke φ_y is

$$\varphi_Y = \frac{\varphi}{2} = \frac{10.6773}{2} = 5.3386\,\mathrm{mWb} \tag{12}$$

The area of the yoke A_y can be set as,

$$A_Y = \frac{A_s}{2} = 2.965925 \times 10^{-3}\,\mathrm{m}^2 \tag{13}$$

The back iron thickness is obtained:

$$C = \frac{A_Y}{L} = \frac{2.965925 \times 10^{-3}}{170 \times 10^{-3}} = 0.01744\,\mathrm{m} \tag{14}$$

The stator pole height H_s is given by,

$$h_s = \frac{D_0}{2} - C - \frac{D}{2} = \frac{171.8}{2} - 17.44 \times 10^{-3} - 44.45 = 24.01\,\mathrm{mm} \tag{15}$$

The rotor pole area A_r is given by

$$\begin{aligned} A_r &= \left(\frac{D}{2} - g\right) \cdot L \cdot \beta_r = \left(\frac{88.9}{2} - 0.5\right) \cdot 170 \times 45^\circ \times \frac{\pi}{180} \\ &= 5.86512 \times 10^{-3}\,\mathrm{m}^2 \end{aligned} \tag{16}$$

The area of the rotor core A_{rc} is given by,

$$A_{rc} = \frac{A_s}{1.6} = 3.707 \times 10^{-3}\,\mathrm{m}^2 \tag{17}$$

The height of the rotor pole h_r is

$$h_r = \frac{D}{2} - g - \frac{D_{sh}}{2} - \frac{A_{rc}}{L} = 14.14\,\mathrm{mm} \tag{18}$$

The average area of A_g is:

$$A_g = 5.898 \times 10^{-3}\,\mathrm{m}^2 \tag{19}$$

The flux density in the air-gap B_g is:

$$B_g = \frac{A_s \cdot B_s}{A_g} = 1.81\,\mathrm{T} \tag{20}$$

The magnetic field intensity of the air-gap H_g is:

$$H_g = \frac{1.81}{4\pi \times 10^{-7}} = 1441346.93\,\frac{\mathrm{AT}}{\mathrm{m}} \tag{21}$$

where AT is ampereturn. The flux density in the yoke B_y is:

$$B_Y = \frac{B_{\max}}{2} = 0.9\,\mathrm{T} \tag{22}$$

The magnetic field intensity of the yoke H_y is obtained from:

$$H_Y = 0.05 \times 10^4\,\frac{\mathrm{AT}}{\mathrm{m}} \tag{23}$$

The flux density in the rotor B_r is:

$$B_r = 0.8 \times B_{\max} = 1.44\,\mathrm{T} \tag{24}$$

The magnetic field intensity of the rotor H_r is obtained from:

$$H_r = 0.25 \times 10^4\,\frac{\mathrm{AT}}{\mathrm{m}} \tag{25}$$

The magnetic field intensity of the rotor core H_{rc} is equal to H_r:

$$H_{rc} = H_r = 0.25 \times 10^4\,\frac{\mathrm{AT}}{\mathrm{m}} \tag{26}$$

The mean path lengths of various sections are given as follows:

$$L_s = h_s + \frac{C}{2} = 24.01 + \frac{17.44}{2} = 32.73\,\mathrm{mm} \tag{27}$$

$$L_g = g = 0.5\,\mathrm{mm} \tag{28}$$

$$L_r = \frac{88.9}{4} - \frac{0.5}{2} + \frac{14.14}{2} - \frac{16}{4} = 43.73\,\mathrm{mm} \tag{29}$$

$$L_{rc} = \pi\,(43.73) = 137.3279\,\mathrm{mm} \tag{30}$$

The mean length L_y for a circular yoke SRM;

$$L_Y = \pi\left[\frac{171.8}{2} - \frac{17.44}{2}\right] = 242.34\,\mathrm{mm} \tag{31}$$

The flux density in the air-gap B_g is given by,

$$B_g = 1.81\,\mathrm{T} \tag{32}$$

The magnetic field intensity of the air-gap H_g is calculated as,

$$H_g = \frac{1.81}{4\pi \times 10^{-7}} = 144.13 \times 10^4\,\frac{\mathrm{AT}}{\mathrm{m}} \tag{33}$$

Using the B-H characteristics for the material used for the laminations, the magnetic field intensity in Ampere-turns per meter for each portion of the machine except the air-gap is obtained. The magnetic field intensities in the stator pole, stator yoke, rotor pole and rotor core are designated as H_s, H_y, H_r and H_{rc}, respectively.

$$B_s = B_{\max} = 1.8\,\mathrm{T}, \qquad H_s = 2 \times 10^4\,\frac{\mathrm{AT}}{\mathrm{m}} \tag{34}$$

$$B_y = \frac{B_{\max}}{2} = 0.9\,\mathrm{T}, \qquad H_y = 0.05 \times 10^4\,\frac{\mathrm{AT}}{\mathrm{m}} \tag{35}$$

$$B_r = 0.8 B_{\max}, \qquad H_r = 0.25 \times 10^4\,\frac{\mathrm{AT}}{\mathrm{m}} \tag{36}$$

$$B_{rc} = B_r, \qquad H_{rc} = 0.25 \times 10^4\,\frac{\mathrm{AT}}{\mathrm{m}} \tag{37}$$

The magnetic circuit equation of the aligned inductance can be written as,

$$\begin{aligned} E &= T_{Ph} \cdot i = 4 \times (H_s \cdot L_s + H_g \cdot L_g + H_r \cdot L_r) + \frac{H_{rc} \cdot L_{rc}}{4} + \frac{H_Y \cdot L_Y}{4} \\ &= 1600.79\,\mathrm{AT} \end{aligned} \tag{38}$$

Now, the total ampere-turns E required for the machine operation at full load can be calculated.

It is also known that $E = T_{Ph} \cdot i$. Since the peak current i_p is assumed initially, the turns per phase can be calculated by;

$$T_{Ph} = \frac{1600.39}{12} = 133.39\,\mathrm{turns} \tag{39}$$

T_{ph} can be calculated. The aligned inductance at maximum current is calculated as,

$$L_{\mathrm{aligned}} = \frac{1600.39 \times 1.8 \times 5.931 \times 10^{-3}}{12^2} = 118.67\,\mathrm{mm} \tag{40}$$

Based on the obtained geometrical and magnetic parameters the SLSRM is modeled and analyzed utilizing 3D-FEM in next parts.

3. THE STRUCTURE OF NOVEL THREE-PHASE SEVEN LAYERS SWITCHED RELUCTANCE MOTOR

The new SLSRM structure is shown in Figure 2. It consists of seven magnetically independent stator and rotor sets. In this structure, each stator set includes four salient poles having 45° arc length with coils wrapped around them. The each set of seven rotor layers comprises of four salient poles with same arc lengths and without windings coils.

The motor volume and dimensions are just like the designed single layer 6/4 SRM but it is divided into 7 slices. Each layer of rotor is 12.7° shifted than another rotor poles which is obtained from:

$$\Delta\theta = \frac{\frac{360}{\text{Stator Poles}}}{\text{Number of Layers}} = \frac{\frac{360}{4}}{7} = 12.7^{\circ} \tag{41}$$

where $\Delta\theta$ is deviation of rotor angle in each layer. As the coils in each layer are turned on together, coils wrapping is safer and also less maintenances is needed because of less isolation problems exiting in usual SRMs construction. Since each stator in the SLSRM has independent phase and all the coils in each layer install to an independent control signal, there is no custom isolation problems which exist in conventional SRMs. This make the SLSRM structure applicable in compare with other types of SRMs. In fact, in this machine can wrap bigger coil which produces higher output torque per volume. The motor assembly of SLSRM is shown in Figures 2(a) and (b). Also, the 3D-FEM model of single layer 6/4 SRM is shown in Figure 3 for comparison study.

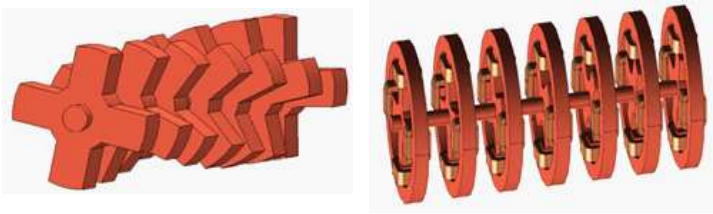

(a) (b)

Figure 2. The assembly of SLSRM: (a) rotor structure, (b) complete assembly (without stack).

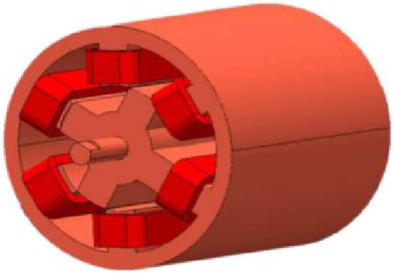

Figure 3. The structure of designed conventional single layer SRM for comparison study.

4. THE COILS ENERGIZING SCHEMATIC

For running the SLSRM, the coils of three stator layers are energized at the same time. Then, this procedure is repeated for other layers, step by step. Always, one of the layers exists that is shared for next strokes. This schematic is continuing for seven steps until 360° rotor rotation. This type of energizing leads to the rotor produces more torque and also decreases the torque ripple.

To study the operation of the novel SLSRM, finding out the region of the rotor firing angle of the layers is significant. On the other hand, the rotor should be in the position which can produce positive torque. If the firing angle of the rotor doesn't choose proper, the negative torque may produce which acts like brake for the motor. As it's explained before, in this seven layers structure, three layers of motor can be energized in order to produce positive torque. These layers should be shifted in compare with the whole layers to produce continuous positive torque. The principle of the operation of this motor is described in Table 1.

Table 1. The energizing principle of the SLSRM.

	Layer 1	**Layer 2**	**Layer 3**	**Layer 4**	**Layer 5**	**Layer 6**	**Layer 7**
Step 1	ON	ON	ON	-	-	-	-
Step 2	-	ON	ON	ON	-	-	-
Step 3	-	-	ON	ON	ON	-	-
Step 4	-	-	-	ON	ON	ON	-
Step 5	-	-	-	-	ON	ON	ON
Step 6	ON	-	-	-	-	ON	ON
Step 7	ON	ON	-	-	-	-	ON

5. FINITE ELEMENT RESULTS AND ANALYSIS

A precise model is needed for the physical motor simulation to incorporate the essential dynamics of the motor [24–29]. The Finite Element Method can be one of the best choices for providing realistic and precise model [30–33]. In this paper, to obtain the field distribution for SLSRM the three-dimensional finite element method (3D-FEM) is used which can be conveniently calculating the motor parameters. The variation energy minimization technique is used to solve for the electric vector potential. This method uses electric vector potential

known as T-Ω formulation which is described in details by authors in the previous papers. The modeling and analysis of the 4/4 SLSRM and the conventional 6/4 SRM are performed by the MagNet CAD package [34]. It should be noted that the machine operates in saturation region for both motor and generator modes, based on its nature.

The magnetic flux density (B) of the proposed SLSRM is obtained and shown in Figure 4 for the beginning of alignment, half aligned and fully aligned positions. For comparative study, the conventional single layer SRM with the same volume and area is also simulated and analyzed by 3D-FEM. The flux density of this 6/4 SRM is illustrated in Figure 5 for unaligned, half aligned and fully aligned positions.

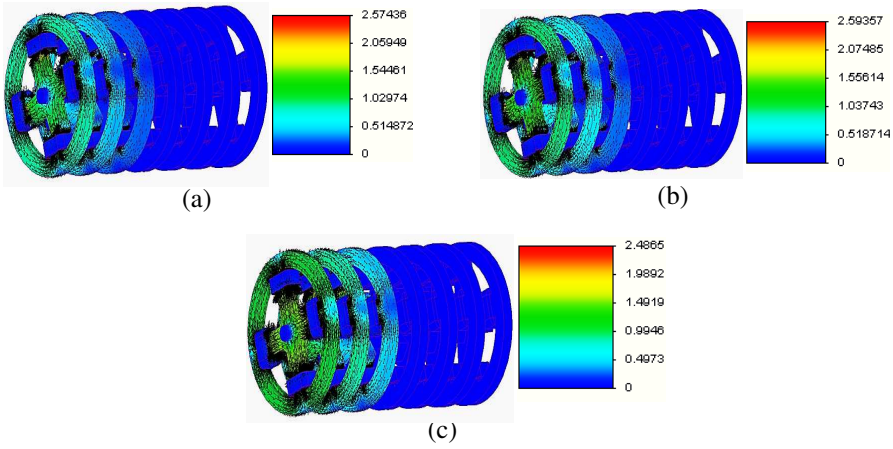

Figure 4. The flux density distribution in the 4/4 SLSRM at: (a) beginning of alignment, (b) half-aligned, (c) fully-aligned.

As illustrated in Figure 4, the maximum value of the flux density (in phase A) is about 2.1 Tesla when three layers are energized, in SLSRM for half-aligned position. In this figure the first shown layer is in the fully aligned position. The second layer is not full aligned yet (half aligned) and the third one is at the first region of alignment (beginning of the alignment). The second and the third layers are turned on in the next step in which another layer is turned on to make the motor have three turned on layers at a moment, again. This process makes a high continues positive torque.

In the conventional single layer SRM the magnitude of the flux density is about 2.38 Tesla for half-aligned position as it's depicted in Figure 5. It means that the SLSRM is able to produce more flux density in comparison with the single layer SRM with same volume in

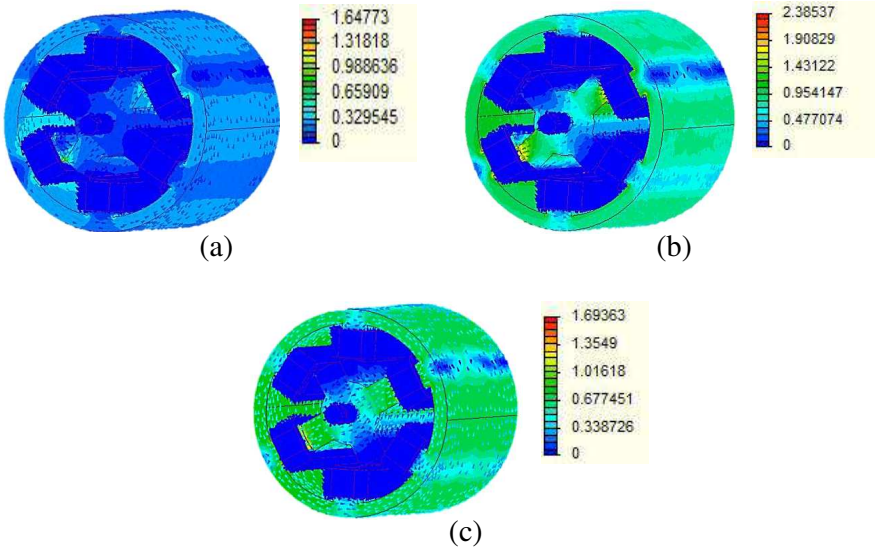

Figure 5. The flux density distribution in the single layer 6/4 SRM at: (a) beginning of alignment, (b) half-aligned, (c) fully-aligned.

identical conditions.

The motor reluctance variation which is the effect of the rotor position variation is a significant parameter and causes the flux variation in rotor and stator poles. The inductance as well as flux linkage profiles are two fundamental characteristic for SRM control. In Figure 6 and Figure 7 the flux linkage of the motor with respect to the rotor position are shown for SLSRM and SRM, respectively.

As depicted in Figure 6, the maximum flux of the novel SLSRM is about 442 mWb at fully aligned, also the minimum flux is about 36 mWb at the beginning of alignment. The flux value is about 42 mWb for half aligned position. However, Figure 7 shows that the maximum flux is about 37 mWb at fully aligned, the minimum flux is about 10 mWb at the beginning of alignment and for half aligned position the flux value is about 27 mWb. From obtained fluxes, it can be resulted that the flux linkage of SLSRM in different rotor positions is higher than conventional SRM. As a summery; the total flux linkage of each phase of SLSRM has 260%, 55% and 19% increase in beginning of alignment, half-aligned, and fully aligned positions, respectively.

For performance evaluation of the two motors, the produced torque could be evaluated in same conditions. In this regard, the produced static torque is obtained (Figure 8) and its shape with respect

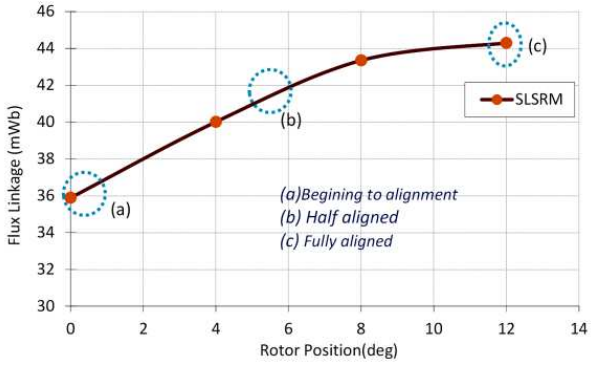

Figure 6. Flux vs. rotor positions in the 4/4 SLSRM.

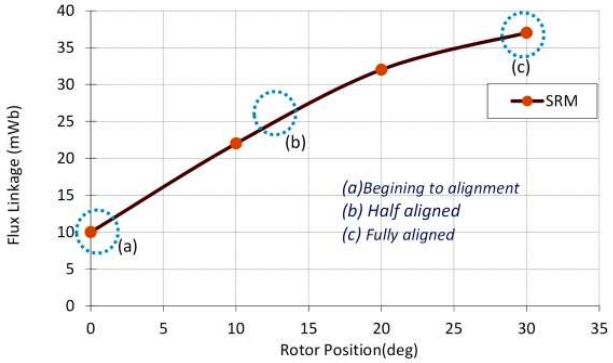

Figure 7. Flux vs. rotor positions in conventional 6/4 SRM.

to the rotor position is shown for the phase current of 3 A and 150 turns coil, from beginning of alignment to fully aligned position. Also, the same curve is obtained for the conventional 6/4 one layer SRM for comparative study and is illustrated in Figure 9.

As depicted in Figure 8, the maximum torque of the novel SLSRM is about 1.3 N·m at half aligned, also the minimum torque is about 0.95 N·m at the beginning of alignment. The torque value is about 0.9 N·m for fully aligned position. However, Figure 9 shows that the maximum torque is about 0.65 N·m at half aligned, the minimum torque is about 0.11 N·m at the beginning of alignment and for fully aligned position the torque value is about 0.01 N·m. Form these results, it can be concluded that the produced torque of SLSRM in different positions is higher than conventional SRM. In fact the output torque of

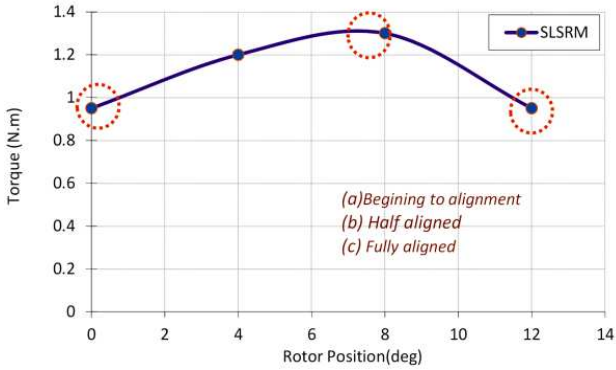

Figure 8. Torque versus rotor positions in the 4/4 SLSRM.

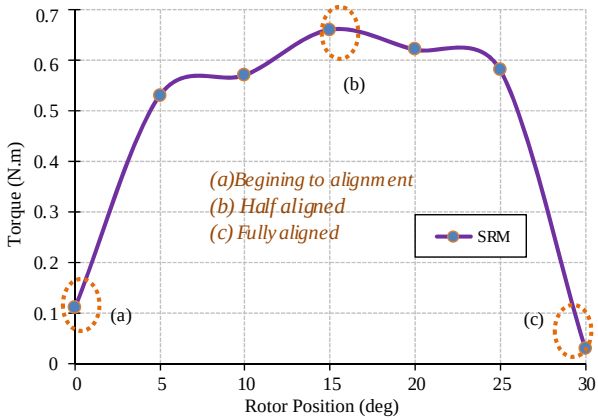

Figure 9. Torque versus rotor positions in conventional 6/4 SRM.

SLSRM has 2, 8.6 and 1.5 times higher value than SRM in half-aligned, beginning of alignment and fully aligned positions, respectively. As stated before, the total volume of both motor is equal; therefore, the torque/volume characteristic of the SLSRM is higher than conventional SRM with noticeable value.

6. CONCLUSION

In this paper, a novel 4 by 4 SRM namely as SLSRM, with seven magnetically independent layers was proposed, analytically designed and modeled utilizing 3D-FEM in various conditions. The comparative

study with a single layer conventional 6/4 SRM were shown that the magnitude of flux density has been faced with an increase in SLSRM. Furthermore, the flux linkage value had 260%, 55% and 19% increase in beginning of alignment, half-aligned, and fully aligned positions, respectively, which shows the increased potential ability of the motor. Moreover, the output torque of SLSRM has 1.5–8.6 times higher value than SRM to prove its high efficiency in same condition The comparative study shows that more than one the layer energizing in SLSRM causes the torque ripple decreases. In addition it was concluded that the torque/volume characteristic of the SLSRM is higher than conventional SRM with noticeable value about twice. This configuration allows more space for coil windings which means users can wrap bigger coil and the motor produces more torque. Moreover, the isolation problem in the coils of layers is also solved and motor cooling is easier.

ACKNOWLEDGMENT

This work was supported by grant from Iran National Science Foundation.

REFERENCES

1. Hasegawa, Y., K. Nakamura, and O. Ichinokura, "A novel switched reluctance motor with the auxiliary windings and permanent magnets," *IEEE Transactions on Magnetics,* Vol. 48, No. 11, 3855–3858, 2012.
2. Torkaman, H. and E. Afjei, "Radial force characteristic assessment in a novel two-phase dual layer SRG using FEM," *Progress In Electromagnetics Research,* Vol. 125, 185–202, 2012.
3. Torkaman, H. and E. Afjei, "Comparison of three novel types of two-phase switched reluctance motors using finite element method," *Progress In Electromagnetics Research,* Vol. 125, 151–164, 2012.
4. Torkaman, H. and E. Afjei, "FEM analysis of angular misalignment fault in SRM magnetostatic characteristics," *Progress In Electromagnetics Research,* Vol. 104, 31–48, 2010.
5. Afjei, E. and H. Torkaman, "The novel two phase field-assisted hybrid SRG: Magnetostatic field analysis, simulation, and experimental confirmation," *Progress In Electromagnetics Research B,* Vol. 18, 25–42, 2009.

6. Baoming, G., A. T. Almeida, and F. Ferreira, "Design of transverse flux linear switched reluctance motor," *IEEE Transactions on Magnetics,* Vol. 45, No. 1, 113–119, 2009.
7. Lim, H., R. Krishnan, and N. S. Lobo, "Design and control of a linear propulsion system for an elevator using linear switched reluctance motor drives," *IEEE Transactions on Industrial Electronics,* Vol. 55, No. 2, 534–542, 2008.
8. Takeno, M., A. Chiba, N. Hoshi, S. Ogasawara, M. Takemoto, and M. A. Rahman, "Test results and torque improvement of the 50-kW switched reluctance motor designed for hybrid electric vehicles," *IEEE Transactions on Industry Applications,* Vol. 48, No. 4, 1327–1334, 2012.
9. Kano, Y., T. Kosaka, and N. Matsui, "Optimum design approach for a two-phase switched reluctance compressor drive," *IEEE Transactions on Industry Applications,* Vol. 46, No. 3, 955–964, 2010.
10. Torkaman, H., E. Afjei, and M. S. Toulabi, "New double-layer-per-phase isolated switched reluctance motor: Concept, numerical analysis, and experimental confirmation," *IEEE Transactions on Industrial Electronics,* Vol. 59, No. 2, 830–838, 2012.
11. Lee, J. W., H. S. Kim, B. Kwon, and B. Taek, "New rotor shape design for minimum torque ripple of SRM using FEM," *IEEE Transactions on Magnetics,* Vol. 40, No. 2, 754–757, 2004.
12. Torkaman, H., E. Afjei, and P. Yadegari, "Static, dynamic, and mixed eccentricity faults diagnosis in switched reluctance motors using transient finite element method and experiments," *IEEE Transactions on Magnetics,* Vol. 48, No. 8, 2254–2264, 2012.
13. Kechroud, A., J. J. H. Paulides, and E. A. Lomonova, "B-spline neural network approach to inverse problems in switched reluctance motor optimal design," *IEEE Transactions on Magnetics,* Vol. 47, No. 10, 4179–4182, 2011.
14. Cai, J., Z. Q. Deng, R. Y. Qi, Z. Y. Liu, and Y. H. Cai, "A novel BVC-RBF neural network based system simulation model for switched reluctance motor," *IEEE Transactions on Magnetics,* Vol. 47, No. 4, 830–838, 2011.
15. Belfore, L. A. and A. A. Arkadan, "A methodology for characterizing fault tolerant switched reluctance motors using neurogenetically derived models," *IEEE Transactions on Energy Conversion,* Vol. 17, No. 3, 380–384, 2002.
16. Torkaman, H. and E. Afjei, "Hybrid method of obtaining degrees of freedom for radial airgap length in srm under normal and faulty conditions based on magnetostatic model," *Progress In*

Electromagnetics Research, Vol. 100, 37–54, 2010.

17. Torkaman, H., E. Afjei, H. Babaee, and P. Yadegari, "A novel method in ACO and its application to rotor position estimation in SRM under normal and faulty conditions," *Journal of Power Electronics,* Vol. 11, No. 6, 856–863, 2011.
18. Nabeta, S. I., I. E. Chabu, L. Lebensztajn, D. A. P. Correa, W. M. Silva, and K. Hameyer, "Mitigation of the torque ripple of a switched reluctance motor through a multiobjective optimization," *IEEE Transactions on Magnetics,* Vol. 44, No. 6, 1018–1021, 2008.
19. Torkaman, H. and E. Afjei, "Sensorless method for eccentricity fault monitoring and diagnosis in switched reluctance machines based on stator voltage signature," *IEEE Transactions on Magnetics,* Vol. 49, No. 2, 912–920, 2013.
20. Afjei, E., M. R. Tavakoli, and H. Torkaman, "Eccentricity compensation in switched reluctance machines via controlling winding turns/stator current: Theory, modeling and electromagnetic analysis," *Applied Computational Electromagnetics Society Journal,* Vol. 28, No. 2, 168–172, 2013.
21. Li, G. J., J. Ojeda, E. Hoang, M. Lecrivain, and M. Gabsi, "Comparative studies between classical and mutually coupled switched reluctance motors using thermal-electromagnetic analysis for driving cycles," *IEEE Transactions on Magnetics,* Vol. 47, No. 4, 839–847, 2011.
22. Du, J., D. Liang, L. Xu, and Q. Li, "Modeling of a linear switched reluctance machine and drive for wave energy conversion using matrix and tensor approach," *IEEE Transactions on Magnetics,* Vol. 46, No. 6, 1334–1337, 2010.
23. Torkaman, H. and E. Afjei, "Comprehensive detection of eccentricity fault in switched reluctance machines using high frequency pulse injection," *IEEE Transactions on Power Electronics,* Vol. 28, No. 3, 1382–1390, 2013.
24. Vaseghi, B., N. Takorabet, and F. Meibody-Tabar, "Transient finite element analysis of induction machines with stator winding turn fault," *Progress In Electromagnetics Research,* Vol. 95, 1–18, 2009.
25. Zhao, W., M. Cheng, R. Cao, and J. Ji, "Experimental comparison of remedial single-channel operations for redundant flux-switching permanent-magnet motor drive," *Progress In Electromagnetics Research,* Vol. 123, 189–204, 2012.
26. Lecointe, J. P., B. Cassoret, and J. F. Brudny, "Distinction of toothing and saturation effects on magnetic noise of induction

motors," *Progress In Electromagnetics Research,* Vol. 112, 125–137, 2011.

27. Touati, S., R. Ibtiouen, O. Touhami, and A. Djerdir, "Experimental investigation and optimization of permanent magnet motor based on coupling boundary element method with permeances network," *Progress In Electromagnetics Research,* Vol. 111, 71–90, 2011.
28. Mahmoudi, A., S. Kahourzade, N. A. Rahim, H. W. Ping, and N. F. Ershad, "Slot-less torus solid-rotor-ringed line-start axial-flux permanent-magnet motor," *Progress In Electromagnetics Research,* Vol. 131, 331–355, 2012.
29. Matyas, A. R., K. A. Biro, and D. Fodorean, "Multi-phase synchronous motor solution for steering applications," *Progress In Electromagnetics Research*, Vol. 131, 63–80, 2012.
30. Wang, Q. and X. Shi, "A an improved algorithm for matrix bandwidth and profile reduction in finite element analysis," *Progress In Electromagnetics Research Letters,* Vol. 9, 29–38, 2009.
31. Tai, C.-C. and Y.-L. Pan, "Finite element method simulation of photoinductive imaging for cracks," *Progress In Electromagnetics Research Letters,* Vol. 2, 53–61, 2008.
32. Mahmoudi, A., N. A. Rahim, and H. W. Ping, "Axial-flux permanent-magnet motor design for electric vehicle direct drive using sizing equation and finite element analysis," *Progress In Electromagnetics Research,* Vol. 122, 467–496, 2012.
33. Tian, J., Z.-Q. Lv, X.-W. Shi, L. Xu, and L. Wei, "An efficient approach for multifrontal algorithm to solve non-positive-definite finite element equations in electromagnetic problems," *Progress In Electromagnetics Research,* Vol. 95, 121–133, 2009.
34. Magnet CAD Package, *User Manual*, Infolytica Corporation Ltd., 2007.